

Hadronic production of $B_s^{(*)}$ at TEVATRON and LHC

Jia-Wei Zhang¹, Zhen-Yun Fang¹, Chao-Hsi Chang^{1,2},

Xing-Gang Wu^{1*}, Tao Zhong¹ and Yao Yu¹

¹*Department of Physics, Chongqing University, Chongqing 400044, P.R. China*

²*Institute of Theoretical Physics, Chinese Academy of Sciences, Beijing 100190, P.R. China*

Abstract

We study the hadronic production of B_s and B_s^* mesons within the fixed-flavor-number scheme, in which the dominant gluon-gluon fusion mechanism is dealt with by using the complete α_s^4 approach. Main theoretical uncertainties for B_s and B_s^* production at TEVATRON and LHC are presented. It is found that when m_s increases by steps of 0.1 GeV, the integrated cross section of $B_s^{(*)}$ decreases by 80% – 100%, when m_b increases by steps of 0.1 GeV, it changes to be $\sim 10\%$. While the uncertainties caused by the parton distribution function and the factorization scale varies within the region of $\frac{1}{5}$ to $\frac{1}{3}$. Considering possible kinematic cut on the transverse momentum and the rapidity cut for the detectors at TEVATRON and LHC, we also make estimations on the B_s and B_s^* production with various kinematic cuts.

PACS numbers: 12.38.Bx, 12.39.Jh, 14.40.Nd, 14.40.Ev.

Keywords: B_s and B_s^* , inclusive hadronic production, uncertainties.

* Email: wuxg@cqu.edu.cn

Since Run II at the TEVATRON Collider started in 2001, the CDF and D0 experiments have successfully collected B_s data [1, 2, 3, 4]. One can use B_s meson to study those interesting topics as QCD model building, physics beyond the Standard Model, the electro-weak symmetry breaking mechanism, charge-parity (CP) violation and etc. [5, 6, 7, 8]. Taking into account the prospects of B_s production at Fermilab TEVATRON and at the newly running CERN LHC, the future numerous data require more accurate theoretical predictions, especially on its hadronic production.

According to the QCD factorization formula, the hadronic production of B_s and B_s^* can be written as

$$d\sigma(S, p_T, \dots) = \sum_{ij} \int \int dx_1 dx_2 F_{H_1, P_1}^i(x_1, \mu_F^2) \cdot F_{H_2, P_2}^j(x_2, \mu_F^2) \cdot d\hat{\sigma}_{ij \rightarrow B_s^{(*)} X}(P_1, P_2, x_1, x_2, \mu_F^2, Q^2, \hat{s}, p_T, \dots), \quad (1)$$

where \sqrt{S} stands for the total collision energy of the incoming hadrons, $F_{H_1, P_1}^i(x_1, \mu_F^2)$ and $F_{H_2, P_2}^j(x_2, \mu_F^2)$ are the parton distribution functions (PDFs) of incoming hadrons H_1 (momentum P_1) and H_2 (momentum P_2) for parton i (with momentum fraction x_1) and parton j (with momentum fraction x_2) respectively. Q^2 is the ‘‘characteristic energy scale of the subprocess squared’’ and μ_F stands for the factorization scale for the PDF and the hard subprocess. A detailed discussion on the choice of Q^2 and μ_F can be found in Ref.[9], here for simplicity, we shall take $Q^2 = \mu_F^2$ for the present perturbative QCD calculation. $d\hat{\sigma}_{ij \rightarrow B_s^{(*)} X}$ stands for the differential cross-section of the relevant hard subprocess, in which $\hat{s} = x_1 x_2 S$ is the c.m.s. energy of the subprocess and P_T is the transverse momentum of $B_s^{(*)}$.

Within the fixed-flavor-number (FFN) scheme [10], where only light quark/antiquark and gluon should be considered in the initial state of the hard scattering subprocess, it can be found that $B_s^{(*)}$ hadronic production are dominated by the gluon-gluon fusion mechanism, which is through the sub-process $g + g \rightarrow B_s^{(*)} + b + \bar{s}$ and is of order α_s^4 . In addition to the gluon-gluon fusion mechanism, there are several different mechanisms for the production, such as that via the quark-antiquark annihilation subprocess $q\bar{q} \rightarrow B_s^{(*)} + b + \bar{s}$ and *etc.* However, it can be found that the contributions to the production from quark-antiquark annihilation are much smaller (only about 1%) than those from gluon-gluon fusion, which is due to the fact that the ‘luminosity’ of gluons is much higher than that of quarks in pp collisions (LHC) and in $p\bar{p}$ collisions (TEVATRON), and there is a suppression factor due to

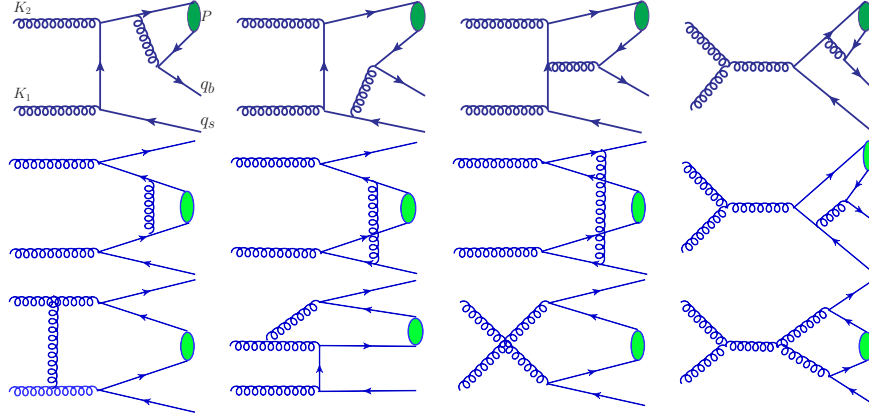


FIG. 1: Typical Feynman diagrams for the hard subprocess $g(K_1)+g(K_2) \rightarrow B_s^{(*)}(P)+\bar{b}(q_b)+s(q_s)$.

the virtual gluon propagator in the annihilation, which is similar to the case of B_c production [11, 12]. Hence in the present letter, we shall concentrate our attention on the gluon-gluon fusion mechanism. And to be useful experimentally, we shall discuss the main uncertainties in estimating the hadronic production of $B_s^{(*)}$, which includes the choices of the factorization energy scale μ_F , the various versions of parton distribution functions (PDFs), the values of the bound state parameters and etc..

As for the dominant gluon-gluon fusion mechanism, its hard subprocess $g + g \rightarrow B_s^{(*)} + b + \bar{s}$ includes 36 Feynman diagrams, whose typical ones are plotted in FIG.1. To derive the analytical squared amplitude for this subprocess is a tedious task, since it contains non-Abelian gluons and massive fermions. Fortunately however, very recently, a generator BCVEGPY [13, 14, 15] for hadronic production of B_c meson has been available, where to deal with the subprocess $g + g \rightarrow B_c + \bar{b} + c$, the so called ‘helicity amplitude approach’ [16, 17]¹ has been adopted to derive analytic expressions at the amplitude level and then do the numerical calculation just at the amplitude level. Here we adopt the same method of Refs.[13, 14, 15] to deal with the present $B_s^{(*)}$ production, which can be obtained by suitable changing the c -quark lines defined in Ref.[13] to the present s -quark lines. To short the paper, we shall only present the main idea on how to deal with those 36 Feynman diagrams based on the ‘helicity amplitude approach’, and the interesting reader may consult Ref.[13] for detailed calculation technology. The main idea is to convert the problem into an equivalent

¹ It should be noted that Ref.[16] presented only the formulae for massless spinor lines, so proper changes as have been done in Ref.[13] should be made so as to deal with the massive spinor lines.

‘massless’ one that is well solved in literature, i.e. by transforming the massive quark lines to be massless ones, and then to apply the symmetries as much as possible. To extend the symmetries for the amplitude corresponding to 36 Feynman diagrams, we first focus on the numerator of the amplitude related to typical fermion lines, and neither consider the color factors nor distinguish the flavor of the fermion lines at the moment. Then, because of Feynman diagram symmetries, these diagrams can be grouped into a few typical ones according to the different type of fermion lines. And then we implement proper factors for the fermion lines: color factors, suitable denominator and spinors and *etc.*, so as to obtain an exact and full typical fermion line that appears in Feynman diagrams. When all kinds of typical fermion line factors, factors for external lines of gluons and gluon propagators are ‘assembled’, then the full term, corresponding to the Feynman diagram of the amplitude, is achieved. Next, to do the phase space integration, we first use RAMBOS [18] routine to generate the requested phase space points and then use VEGAS [19] program to perform the integrations.

Based on the above calculation technology, we present the numerical results. As for the present LO estimation, f_{B_s} appears in the amplitude as a linear factor, so the production cross sections are proportional to it squared. Therefore, the uncertainties in the production from f_{B_s} can be figured out straightforwardly, so throughout the paper, we take $f_{B_s} = 0.209$ GeV[20]. And because the spin splitting effects are ignored here, so there is no difference for the decay constant between the spin stats [1S_0] and [3S_1]. Further more, we shall study the uncertainties in ‘a factorization way’ throughout the paper, i.e., all of the parameters vary independently in their reasonable regions. For instance, when focussing on the uncertainties from the constitute s -quark mass m_s , we let it be a basic ‘input’ parameter varying in a possible range

$$0.4\text{GeV} \leq m_s \leq 0.7\text{GeV}, \quad (2)$$

with all the other factors, including the B_s -meson mass, the decay constant f_{B_s} and *etc.* being fixed.

In TAB.I, we show the uncertainties from m_s , where the other factors are fixed precisely as: $m_b = 4.9$ GeV, the PDFs are taking as CTEQ6L [23]; the strong coupling α_s is in LO and the factorization energy scale is taken to be $\mu_F^2 = p_{T_{B_s}}^2 + m_{B_s}^2$. Note that for the mass of B_s , the experimental result is $m_{B_s} = 5.3663 \pm 0.0006$ GeV [21], while the prediction by

TABLE I: Total cross section for the hadronic production of $B_s[1^1S_0]$ and $B_s^*[1^3S_1]$ with varying m_s , where $m_b = 4.9$ GeV, $m_{B_s} = m_s + m_b$, the gluon distribution function is taken from CTEQ6L, $\mu_F^2 = p_{T_{B_s}}^2 + m_{B_s}^2$ and α_s is of leading order.

| - | TEVATRON($\sqrt{S} = 1.96$ TeV) | | | | LHC ($\sqrt{S} = 14.$ TeV) | | | |
|-----------------------|----------------------------------|-------|-------|-------|-----------------------------|-------|-------|-------|
| m_s (GeV) | 0.4 | 0.5 | 0.6 | 0.7 | 0.4 | 0.5 | 0.6 | 0.7 |
| σ_{B_s} (nb) | 48.25 | 24.43 | 14.33 | 9.326 | 512.6 | 262.2 | 155.1 | 101.5 |
| $\sigma_{B_s^*}$ (nb) | 165.5 | 82.18 | 46.78 | 29.30 | 1739. | 871.8 | 500.5 | 316.2 |

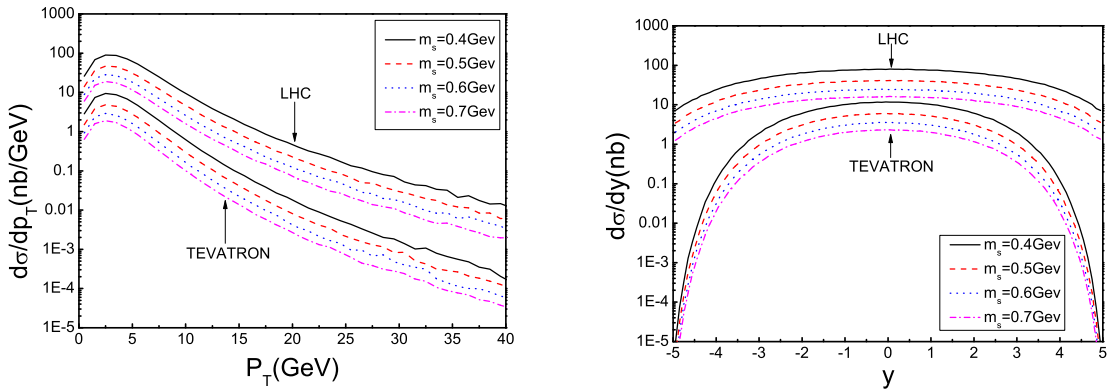


FIG. 2: B_s differential distributions versus its P_T and rapidity y with varying m_s . The gluon distribution function is taken from CTEQ6L, the characteristic energy scale is taken as $Q^2 = p_{T_{B_s}}^2 + m_{B_s}^2$, and α_s is of leading order. The solid line, dashed line, dotted line and dash-dot line stands for $m_s = 0.4, 0.5, 0.6$ and 0.7 GeV respectively. The upper (lower) four lines corresponding to the distributions at LHC (TEVATRON) respectively.

lattice QCD is about 5.37 GeV [22]. Thus with $m_b = 4.9$ GeV and $m_{B_s} = m_b + m_s$ ², the obtained m_{B_s} is in the region of theoretical prediction as well as experimental measurement. In Table I, the total cross-section for the hadronic production of $B_s[1^1S_0]$ and $B_s^*[1^3S_1]$ at TEVATRON and LHC are computed. From TAB.I, one may observe that the total cross

² This relation should be satisfied according to the gauge invariance of the hard subprocess. Further more, at the present, we treat B_s as non-relativistic and weak binding state, then at LO the relative momentum between the constitute quarks can be ignored.

TABLE II: Total cross section for the hadronic production of $B_s[1^1S_0]$ and $B_s^*[1^3S_1]$ with various m_b , where m_s is fixed to be 0.5 GeV, the gluon distribution function is taken from CTEQ6L, the factorization energy scale is chosen $\mu_F^2 = p_{T_{B_s}}^2 + m_{B_s}^2$ and α_s is of leading order.

| - | TEVATRON($\sqrt{S} = 1.96$ TeV) | | | LHC ($\sqrt{S} = 14.$ TeV) | | |
|----------------------|----------------------------------|-------|-------|-----------------------------|-------|-------|
| m_b (GeV) | 4.8 | 4.9 | 5.0 | 4.8 | 4.9 | 5.0 |
| $\sigma_{B_s}(nb)$ | 22.60 | 24.43 | 26.49 | 280.9 | 262.2 | 245.7 |
| $\sigma_{B_s^*}(nb)$ | 88.86 | 82.18 | 76.09 | 818.1 | 871.8 | 929.3 |

section of $B_s^*[1^3S_1]$ is about 3 times bigger that of $B_s[1^1S_0]$, which roughly agree with the naive counting of spin states. m_s affects the total cross section greatly, e.g. when m_s increases by steps of 0.1 GeV, then the cross section of B_s or B_s^* decreases by about 80% – 100%. To show this point more clearly, we draw the B_s - P_T and rapidity Y distributions with $m_s = 0.4, 0.5, 0.6$ and 0.7 GeV respectively in FIG.2. This implies that the present treatment of s-quark as heavy quark is reasonable but may be not too accurate, and a more accurate one, e.g. by including proper relativistic effects into the bound state, maybe improve the estimation, which is out of the range of the present letter. A similar calculation by varying m_b within its reasonable region but with fixed $m_s = 0.5$ GeV, as shown by TAB.II, which shows that when m_b increases by steps of 0.1 GeV, the cross section of B_s or B_s^* changes slightly, which is around 10%. More precise values of m_b and m_s from potential model or lattice QCD can make the our estimations more reliable. In the following parts of the paper when examining the uncertainties from other factors, we shall always take the center values of $m_s = 0.5$ GeV and $m_b = 4.9$ GeV, for the quark masses.

PDF is of non-perturbative nature, which can be obtained through global fitting of the experimental data. Here we take CTEQ6L [23] and MRST2001L[24] as typical examples to study the uncertainty caused by PDF. As shown in Eq.(1) PDF can be factorized out at the energy scale μ_F^2 with the help of pQCD factorization theorem. The factorization scale μ_F^2 can be usually taken as the characteristic energy scale for the hard subprocess (Q^2), i.e. $\mu_F^2 = Q^2$. For the present case, the gluon-gluon fusion subprocess is of three-body final state and contain heavy quarks, so there are ambiguities in choosing Q^2 and various choices of Q^2 would generate quite different results. Since such kind of ambiguity cannot be justified

TABLE III: Total cross-section for the hadronic production of $B_s[1^1S_0]$ and $B_s^*[1^3S_1]$ at TEVATRON and at LHC with LO running α_s and the characteristic energy scale Type A: $Q^2 = \hat{s}/4$; Type B: $Q^2 = p_T^2 + m_{B_s}^2$ and Type C: $Q^2 = p_{Tb}^2 + m_b^2$.

| - | TEVATRON($\sqrt{S} = 1.96$ TeV) | | | | LHC($\sqrt{S} = 14.$ TeV) | | | |
|----------------------|----------------------------------|--------|----------|--------|----------------------------|--------|-----------|--------|
| - | CTEQ6L | CTEQ6L | MRST2001 | CTEQ6L | CTEQ6L | CTEQ6L | MRST2001L | CTEQ6L |
| Q^2 | Type A | Type B | | Type C | Type A | Type B | | Type C |
| $\sigma_{B_s}(nb)$ | 17.55 | 24.43 | 20.82 | 25.01 | 203.5 | 262.3 | 221.7 | 264.1 |
| $\sigma_{B_s^*}(nb)$ | 58.37 | 82.19 | 69.83 | 83.89 | 675.8 | 871.8 | 734.2 | 876.5 |

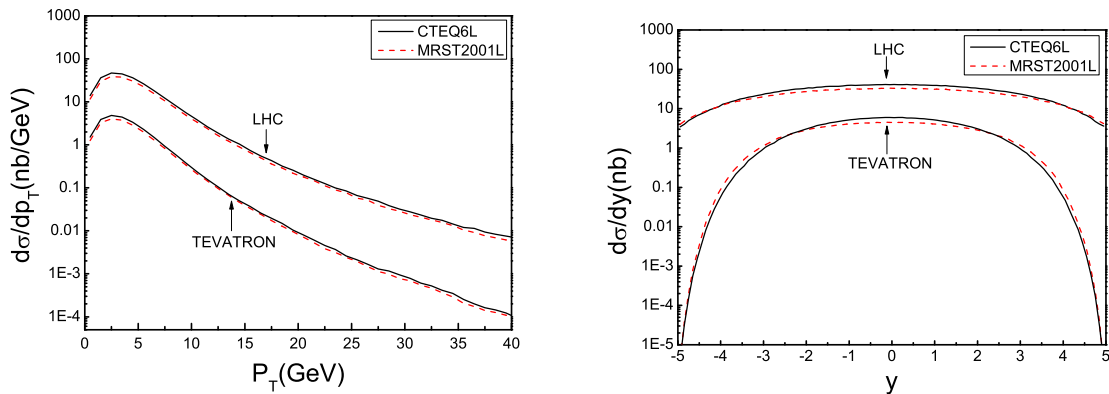


FIG. 3: B_s differential distributions versus its transverse momentum P_T and rapidity y for different LO PDFs, where the solid line and the dashed line are for CTEQ6L and MRST2001L respectively. The characteristic energy scale is taken as $Q^2 = p_T^2 + m_{B_s}^2$. The upper and lower two lines corresponding to the distributions in LHC and TEVATRON accordingly.

by the LO calculation itself, so we take it as the uncertainty of the LO calculation. In the following we choose three typical examples to study this kind of uncertainties: Type A: $Q^2 = \hat{s}/4$, the C.M. energy squared of the subprocess that is divided by 4; Type B: $Q^2 = p_T^2 + m_{B_s}^2$, the transverse mass squared of the B_s meson; and Type C: $Q^2 = p_{Tb}^2 + m_b^2$, the transverse mass squared of the b quark. For comparison between TEVATRON and LHC and to pinpoint the uncertainties from PDFs, α_s running and the choices of the characteristic energy scale Q^2 , we calculate the production cross sections according to two types of PDFs,

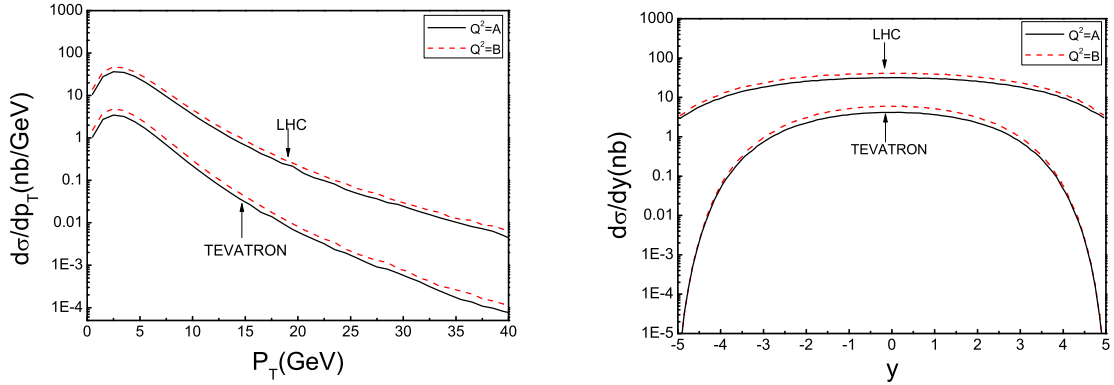


FIG. 4: B_s differential distributions versus its transverse momentum p_T and rapidity y for typical choices of Q^2 , where the solid and the dashed lines are for Type A and Type B respectively. The gluon distribution is chosen as CTEQ6L and the running α_s is in leading order. The upper and lower two lines corresponding to the distributions in LHC and TEVATRON accordingly.

the strong coupling α_s fixed by the corresponding PDFs and the characteristic Q^2 chosen as Type A, Type B and Type C. The obtained results are shown in TAB III. From TABLE III, it is found that the difference caused by the two LO PDFs is small, which is $\sim 15\%$. The choice of Q^2 as Type A and Type B cause changes is somewhat larger, i.e. $20\% - 30\%$, while the choose of Type B and Type C leads to negligible changes to the cross section (less than 1%). The total cross section of the $B_s^{(*)}$ production at LHC are at least one order larger in magnitude than that at TEVATRON. This is mainly due to the fact that LHC ($\sqrt{S} = 14$. TeV) has much higher collide energy than TEVATRON ($\sqrt{S} = 1.96$ TeV), so the lowest boundary of the gluon momentum fractions x_i ($i = 1, 2$) at LHC are much smaller than that at TEVATRON and then there are more interacting gluons that have a C.M. energy above the threshold for the subprocess, in the collision hadrons at LHC than at TEVATRON. This can be shown more clearly by the p_T and y differential cross sections. More explicitly, we draw the curves for pseudo-scalar meson B_s in FIGS.(3,4). FIG.3 shows that the differential distributions for the two PDFs CTEQ6L and MRST2001L and FIG.4 shows that the differential distributions for the two Q^2 Type A and Type B. In regions of comparatively small p_T and $|y|$, the distributions of MSRT2001L are smaller than that of CTEQ6L. From the figure, we also see that the p_T distributions in TEVATRON are steeper than those in LHC. From TABLE III, we know that changes in the cross section caused by

TABLE IV: Dependence of $R = \left(\frac{\sigma_{TEVTRON}}{\sigma_{LHC}}\right)$ on P_{Tcut} for $B_s[1^1S_0]$ and $B_s^*[1^3S_1]$.

| - | B_s | | | | | B_s^* | | | | |
|---------------------|-------|------|------|------|------|---------|------|------|------|------|
| $P_{Tcut}(GeV)$ | 0 | 5 | 20 | 35 | 50 | 0 | 5 | 20 | 35 | 50 |
| $R(\times 10^{-2})$ | 9.32 | 7.71 | 3.00 | 1.67 | 0.70 | 9.43 | 7.80 | 3.12 | 1.85 | 0.87 |

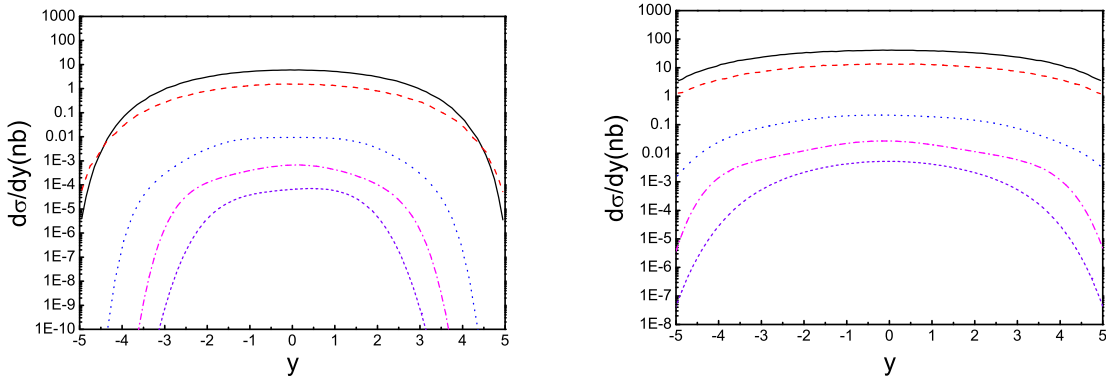


FIG. 5: B_s differential distributions versus its y with various p_{Tcut} in TEVATRON (left diagram) and in LHC (right diagram). Solid line corresponds to the full production without p_{Tcut} ; dashed line to $p_{Tcut} = 5.0$ GeV; dot line to $p_{Tcut} = 20.0$ GeV; the dash-dot line to $p_{Tcut} = 35.0$ GeV; the short dash line to $p_{Tcut} = 50.0$ GeV .

Type B and Type C is quite small (less than 1%), and the curves of the production obtained by Type B and Type C are almost overlap, so we do not draw the curves for Type C.

Experimentally, when the produced B_s and B_s^* mesons with a small P_T or a large rapidity y are too close to the collision beam, they cannot be measured, so only ‘detectable’ events should be taken into account, i.e. events with proper kinematic cuts on P_T and y should be properly set in the estimates. As a comparison, we define a ratio $R = \left(\frac{\sigma_{TEVATRON}}{\sigma_{LHC}}\right)_{P_{Tcut}}$ to show how P_{Tcut} affects the integrated cross sections at TEVATRON and LHC, and the results is shown in TAB.IV. It can be found that without P_{Tcut} , the integrated cross section at LHC is about one order higher than that at TEVATRON, and the value of R decreases greatly with the increment of P_{Tcut} , at about $P_{Tcut} \simeq 45$ GeV, $R \sim 1$.

Next, as an explicit example to show how the different cuts affect the production, we study

TABLE V: Values of $R_{P_{Tcut}}$ for the hadronic production of pseudo-scalar B_s meson in TEVATRON and LHC.

| P_{Tcut} | 0.0 GeV | | | 5 GeV | | | 20 GeV | | | 35 GeV | | | 50 GeV | | |
|---------------------------|---------|------|------|-------|------|------|--------|------|------|--------|------|------|--------|------|------|
| y_{cut} | 1.0 | 1.5 | 2.0 | 1.0 | 1.5 | 2.0 | 1.0 | 1.5 | 2.0 | 1.0 | 1.5 | 2.0 | 1.0 | 1.5 | 2.0 |
| $R_{P_{Tcut}}$ (TEVATRON) | 0.47 | 0.66 | 0.80 | 0.48 | 0.67 | 0.81 | 0.59 | 0.79 | 0.92 | 0.68 | 0.86 | 0.95 | 0.69 | 0.92 | 0.99 |
| $R_{P_{Tcut}}$ (LHC) | 0.32 | 0.47 | 0.60 | 0.33 | 0.48 | 0.61 | 0.40 | 0.57 | 0.71 | 0.45 | 0.62 | 0.77 | 0.56 | 0.73 | 0.83 |

the distributions of P_T and y for B_s . For the present purpose, we take CTEQ6L for PDF, LO running α_s and Type B energy scale to carry out the study. The correlations between P_T and y are interesting, so we plot the y -distributions with various P_T -cuts over a wide range $P_{Tcut} : 5.0 \sim 35$ GeV in FIG.5. FIG.5 shows that the dependence of the differential distributions on rapidity y with different P_{Tcut} at LHC exhibits a broader profile than that at TEVATRON. The p_T -distributions of the production vary with y_{cut} mainly due to the fact that as p_T increases, the dependence of the distribution on y becomes smaller as the value of y_{cut} becomes less important. To analyze the quantitative difference of the differential distributions with regard to P_{Tcut} and y_{cut} , we introduce a ratio for the integrated hadronic cross sections, $R_{P_{Tcut}} = \left(\frac{\sigma_{y_{cut}}}{\sigma_0} \right)_{P_{Tcut}}$, where $\sigma_{y_{cut}}$ and σ_0 are the hadronic cross section with and without y_{cut} respectively. The ratio $R_{P_{Tcut}}$ varies with p_{Tcut} and y_{cut} , and its values are given in TAB.V. TAB.V shows that for a fixed y_{cut} , the value of $R_{P_{Tcut}}$ becomes larger with increasing P_{Tcut} . It is understandable that the differential distributions versus the rapidity y decrease with the increment of P_T , so the contributions to the hadronic cross section surviving after the cut, i.e. ($|y| \leq y_{cut}$), increase with the increment of P_{Tcut} .

To summarize: We have presented quantitative studies on the uncertainties in estimates of the $B_s^{(*)}$ meson hadronic production within the FFN scheme. The investigated quantitatively uncertainties involve the PDF, the values of m_b and m_s , and the characteristic energy scale Q^2 of the process and etc.. It is found that when m_s increases by steps of 0.1 GeV, the integrated cross section of $B_s^{(*)}$ decreases by about 80%–100%, when m_b increases by steps of 0.1 GeV, it is about 10%. While the uncertainties caused by the parton distribution function and the factorization scale varies within the region of $\frac{1}{5}$ to $\frac{1}{3}$. We have also shown the

differences between LHC and TEVATRON for various observable with reasonable kinematic cuts, such as the cuts on the $B_s^{(*)}$ meson transverse momentum P_{Tcut} and rapidity y_{cut} . Our results show that the experimental studies of the $B_s^{(*)}$ meson at the two colliders are complimentary and stimulative. Concerning the prospects of B_s production at Fermilab TEVATRON and at CERN LHC, the obtained results may be as useful references for these experiments. Since LHC has much higher luminosity and higher collision energy than that of TEVATRON, it seems that the particularly interesting topics on B_s may be more accessible and fruitful at LHC than that at TEVATRON. Further more, it is reasonable to assume that, similar to the hadronic production of J/Ψ , B_c and Ξ_{cc} [25, 26, 27], the ‘heavy quark mechanisms’ via the sub-processes $g + s \rightarrow B_s^{(*)} + \dots$ and $g + \bar{b} \rightarrow B_s^{(*)} + \dots$ may be as important as the gluon-gluon fusion mechanism, which should be treated on the equal footing in comparison to that of the gluon-gluon fusion mechanism. However to be consistent theoretically and to deal with the possible double counting from all these mechanisms, one should work in the general-mass variable-flavor-number (GM-VFN) scheme [28, 29, 30] in stead of the FFN scheme. A detailed discussion on the GM-VFN scheme, and a comparison of $B_s^{(*)}$ production within these two schemes is in preparation and shall be presented elsewhere.

Acknowledgments: This work was supported in part by Natural Science Foundation Project of CQ CSTC under Grant No.2008BB0298 and Natural Science Foundation of China under Grant No.10805082 and No.10875155, and by the grant from the Chinese Academy of Engineering Physics under Grant No.2008T0401 and Grant No.2008T0402.

-
- [1] D. Acosta *et al.*, CDF Collaboration, Phys.Rev. D**71**, 032001 (2005); Phys.Rev. Lett.**94**, 101803 (2005); T. Aaltonen *et al.*, CDF Collaboration, Phys.Rev. Lett.**100**, 082001(2008);
 - [2] A. Abulencia *et al.*, CDF Collaboration, Phys.Rev. Lett.**97**, 062003 (2006); Phys.Rev. Lett. **97**, 242003(2006) ;
 - [3] V.M. Abazov *et al.*, D0 Collaboration, Phys.Rev. Lett.**94**, (2005) 042001; Phys.Rev. Lett.**98**, (2007)121801;
 - [4] H.G. Evans, arXiv:0705.4598; S. Burdin, arXiv:0707.1509;

- [5] A. Deandrea, N.Di Bartolomeo, R. Gatto and G. Nardulli, Phys.Lett. **B318**, 549(1993); G. Hiller and E.O. Iltan, Phys.Lett. **B409**, 425(1997).
- [6] I. Dunietz, R. Fleischer and U. Nierste, Phys.Rev. **D63**, 114015(2001); S.P.Baranov, Phys.Atom.Nucl.**65**, 879 (2002).
- [7] T.M. Aliev and M. Savci, Phys.Rev. **D73**, 114010(2006); T.M. Aliev, K. Azizi and A. Ozpineci, Eur.Phys.J. **C51**, 593(2007).
- [8] J.R. Catmorea, Nucl.Phys. B(Proc. Suppl.)**167**, 237(2007); B.A. Kniehl, G. Kramer, I. Schienbein, H. Spiesberger, Phys. Rev. **D77**, 014011(2008); S. Stone and L. Zhang, arXiv:0812.2832; B.A. Kniehl, arXiv:0807.2215.
- [9] M. Klasen, B.A. Kniehl, L.N. Mihaila and M. Steinhauser, Phys. Rev. Lett. **89**, 032001(2002).
- [10] W. Beenakker, H. Kuijf, W.L. van Neerven and J. Smith, Phys.Rev. **D40**, 54(1989); P. Nason, S. Dawson and R.K. Ellis, Nucl.Phys. **B327**, 49(1989);
- [11] Chao-Hsi Chang and Yu-Qi Chen, Phys. Rev. D **48**, 4086 (1993).
- [12] Chao-Hsi Chang and Xing-Gang Wu, Eur. Phys. J. C **38**, 267 (2004).
- [13] Chao-Hsi Chang, Chafik Driouich, Paula Eerola and Xing-Gang Wu, Comput.Phys.Commun. **159**, 192(2004).
- [14] Chao-Hsi Chang, Jian-Xiong Wang, and Xing-Gang Wu, Comput.Phys.Commun. **174**, 241(2006).
- [15] Chao-Hsi Chang, Jian-Xiong Wang, and Xing-Gang Wu, Comput.Phys.Commun. **175**, 624(2006).
- [16] R. Kleiss and W.J. Stirling, Nucl.Phys. **B262**, 235(1985).
- [17] Z. Xu, D.H. Zhang and L. Chang, Nucl.Phys. **B291**, 392(1987).
- [18] R. Kleiss and W.J. Stirling, Comput. Phys. Commun, **40**, 359(1986).
- [19] G.P. Lepage, J. Comp. Phys **27**, 192(1978).
- [20] P. Colangelo and A. Khodjamirian, ‘At the Frontier of Particle Physics. Handbook of QCD’, Edited by M. Shifman and B. Ioffe, World Scientific, Singapore (2001), p.1495.
- [21] C. Amsler *et al.*, Particle Data Group, Phys.Lett. **B667**, 1(2008).
- [22] E. B. Gregory *et al.*, HPQCD Collaboration, arXiv: 0810.1845.
- [23] H.L. Lai, et al.JHEP**0207**, 012 (2002).
- [24] A.D. Martin, R.G. Roberts, W.J. Stirling and R.S. Thorne, Eur. Phys. J. **C23**, 73(2002).
- [25] Cong-Feng Qiao, J.Phys. **G29**, 1075(2003), hep-ph/0202227.

- [26] Chao-Hsi Chang, Cong-Feng Qiao, Jian-Xiong Wang and Xing-Gang Wu, Phys.Rev. **D73**, 094022(2006).
- [27] Chao-Hsi Chang, Jian-Ping Ma, Cong-Feng Qiao and Xing-Gang Wu, J. Phys. G: Nucl. Part. Phys. **34**, 845(2007); Chao-Hsi Chang, Jian-Xiong Wang and Xing-Gang Wu, Comput.Phys. Commun.**177**, 467(2007).
- [28] F.I. Olness, R.J. Scalise and W.K. Tung, Phy. Rev. **D59**, 014506(1998).
- [29] M.A.G. Aivazis, J.C. Collins, F.I. Olness and W.K. Tung, Phys. Rev. **D50**, 3102(1994); M.A.G. Aivazis, F.I. Olness and W.K. Tung, Phys. Rev. **D50**, 3085(1994).
- [30] J. Amundson, C. Schmidt, W.K. Tung and X.N. Wang, JHEP10, 031(2000).